JGR Oceans

RESEARCH ARTICLE
10.1029/2024JC021586

Using DIC-$\delta^{13}C$ Pair to Constrain Anthropogenic Carbon Increase in the Southeastern Atlantic Ocean Over the Most Recent Decade (2010–2020)

Hui Gao[1,2], Meibing Jin[3,4], Hui Zhao[2], Najid Hussain[1], and Wei-Jun Cai[1]

[1]School of Marine Science and Policy, University of Delaware, Newark, DE, USA, [2]College of Chemistry and Environmental Science, Guangdong Ocean University, Zhanjiang, China, [3]School of Marine Sciences, Nanjing University of Information Science and Technology, Nanjing, China, [4]International Arctic Research Center, Fairbanks, AK, USA

Key Points:

- Anthropogenic carbon uptake rate estimated from $\delta^{13}C$ matches with that from dissolved inorganic carbon except in the surface in the southeastern Atlantic Ocean
- Anthropogenic carbon changes exhibit significant vertical variations depending on water masses and circulation
- Anthropogenic carbon increase rate during 2010–2020 has accelerated ~19% from that during 1983/84–2010 in the study region

Supporting Information:

Supporting Information may be found in the online version of this article.

Correspondence to:

W.-J. Cai,
wcai@udel.edu

Citation:

Gao, H., Jin, M., Zhao, H., Hussain, N., & Cai, W.-J. (2024). Using DIC-$\delta^{13}C$ pair to constrain anthropogenic carbon increase in the southeastern Atlantic Ocean over the most recent decade (2010–2020). *Journal of Geophysical Research: Oceans*, *129*, e2024JC021586. https://doi.org/10.1029/2024JC021586

Received 15 JUL 2024
Accepted 19 OCT 2024

Author Contributions:

Conceptualization: Hui Gao, Wei-Jun Cai
Data curation: Najid Hussain, Wei-Jun Cai
Formal analysis: Hui Gao, Meibing Jin, Hui Zhao, Wei-Jun Cai
Funding acquisition: Wei-Jun Cai
Investigation: Hui Gao, Meibing Jin, Wei-Jun Cai
Methodology: Hui Gao, Meibing Jin, Hui Zhao, Wei-Jun Cai
Project administration: Wei-Jun Cai
Resources: Wei-Jun Cai
Software: Hui Gao, Meibing Jin
Supervision: Wei-Jun Cai
Validation: Hui Gao, Wei-Jun Cai
Visualization: Hui Gao, Meibing Jin, Wei-Jun Cai
Writing – original draft: Hui Gao
Writing – review & editing: Hui Gao, Meibing Jin, Hui Zhao, Wei-Jun Cai

Abstract The southeastern Atlantic Ocean is a crucial yet understudied region for the ocean absorption of anthropogenic carbon (C_{anth}). Data from the A12 (2020) and A13.5 (2010) cruises offer an opportunity to examine changes in dissolved inorganic carbon (DIC), its stable isotope ($\delta^{13}C$), and C_{anth} over the past decade within a limited region (1~3°E, 32~42°S). For the decade of 2010–2020, C_{anth} invasion was observed from the sea surface down to 1,200 m based on both DIC and $\delta^{13}C$ data. The mean C_{anth} increase rate (1.08 ± 0.26 mol m^{-2} yr^{-1}) during this period accelerated from 0.87 ± 0.05 mol m^{-2} yr^{-1} during the previous period (1983/84–2010). The $\delta^{13}C$-based C_{anth} increase closely matches the DIC-based estimation below 500 m but is 26% higher in the upper ocean. This discrepancy is likely due to $\delta^{13}C$'s longer air-sea exchange timescale, seasonal variability in the upper ocean, and the chosen ratio of anthropogenically induced changes in $\delta^{13}C$ and DIC. Finally, column inventory changes based on the two methods also exhibit very similar mean C_{anth} uptake rates. The paired DIC concentration and stable isotope dataset may enhance our ability to constrain C_{anth} accumulation and its controlling mechanisms in the ocean.

Plain Language Summary The stable carbon isotope signal ($\delta^{13}C$) of oceanic dissolved inorganic carbon (DIC) is a sensitive tracer for the absorption of anthropogenic carbon from the atmosphere. We collected $\delta^{13}C$ data from a limited region in the southeastern Atlantic Ocean and used them to examine the anthropogenic carbon changes over the most recent decade. From 2010 to 2020, anthropogenic carbon invasion can be found from the sea surface to a depth of 1,200 m with an accelerated increase rate compared to the period from 1983/84 to 2010. The $\delta^{13}C$-based estimation of anthropogenic carbon increase matches closely with the DIC-based estimation below 500 m but is significantly higher in the upper ocean. This discrepancy likely arises from differences in equilibrium timescales, the ratio of the anthropogenic $\delta^{13}C$/DIC change, and different influences by seasonal variability in the upper ocean. Nonetheless, the entire water column inventory changes based on both two methods show very close mean anthropogenic carbon uptake rates.

1. Introduction

Since the Industrial Revolution, human activities have significantly increased carbon dioxide (CO_2) concentrations in the atmosphere. Oceanic uptake of anthropogenic CO_2 or carbon (C_{anth}) has played an important role in slowing down atmospheric CO_2 increase and thus the global warming potential (Friedlingstein et al., 2022; Sabine et al., 2004). The rate of oceanic C_{anth} accumulation is estimated mainly based on the temporal variation of dissolved inorganic carbon (DIC) (Brewer, 1978; Chen & Millero, 1979; Friis et al., 2005; Gruber et al., 1996; Touratier & Goyet, 2004; Vázquez-Rodríguez et al., 2009). Quay et al. (1992) proposed a method that utilizes the $^{13}C/^{12}C$ isotope ratio of DIC (hereafter referred to as $\delta^{13}C$, in per mil, ‰) to estimate ocean uptake of C_{anth} based on the concept that fossil fuel burning and terrestrial biomass loss continuously add ^{13}C depleted CO_2 into the atmosphere and lower its $\delta^{13}C$, a process known as the atmospheric ^{13}C Suess effect (Keeling, 1979). Thus, the C_{anth} fraction of DIC in the ocean can be estimated by observing the temporal changes of the isotopic signal (to a more negative value) of the ocean DIC pool due to the uptake of CO_2, a phenomenon also known as the oceanic ^{13}C Suess effect (Eide et al., 2017; Körtzinger et al., 2003; Olsen et al., 2006; Quay et al., 1992, 2007, 2017).

Decadal C_{anth} changes have been investigated in the global ocean (Gruber, Clement, et al., 2019; Müller et al., 2023; Sabine et al., 2004) and within individual ocean basins, including the Atlantic Ocean (Gao et al., 2022; Körtzinger et al., 2003; Quay et al., 2007; Wanninkhof et al., 2010; Woosley et al., 2016), the Pacific

Ocean (Carter et al., 2019; Quay et al., 2017; Sonnerup et al., 2007), the Indian Ocean (Sabine et al., 1999; Williams et al., 2021), and the Southern Ocean (McNeil et al., 2001; Pardo et al., 2014) by reoccupations of the World Ocean Circulation Experiment/Joint Global Ocean Flux Study (WOCE/JGOFS) and Global Ocean Ship-based Hydrographic Investigations Program (GO-SHIP) sections. The Southern Ocean has absorbed and stored a disproportionate amount of C_{anth}, estimated at 40% of the total C_{anth} inventory (Gruber, Landschützer, & Lovenduski, 2019; Landschützer et al., 2015; Sallée et al., 2012). Although the South Atlantic Ocean is considered a significant C_{anth} sink, with 3–4 Pg C decade^{-1} uptake rate (Gao et al., 2022; Wanninkhof et al., 2010; Woosley et al., 2016), the C_{anth} changes in the southeastern Atlantic Ocean have been understudied due to a lack of observational data.

Both DIC and $\delta^{13}C$ in the ocean are affected by multiple physical and biogeochemical processes, such as ocean mixing, biological production, degradation of organic matter, the formation or dissolution of calcium carbonate, and air-sea CO_2 exchange (Schmittner et al., 2013). Therefore, using both DIC and $\delta^{13}C$ data sets, rather than DIC alone, to estimate C_{anth} can provide a more comprehensive understanding of carbon sources and cycling processes in oceanic environments. Observations along the GO-SHIP line A12 in March 2020 (an incomplete A13.5 transect) offer an opportunity to explore changes in C_{anth} over the most recent decade together with $\delta^{13}C$, DIC, and hydrographic data collected along a nearly identical transect (A13.5) in 2010 between 42° and 32°S. Although there were fewer stations in 2020 compared to 2010 due to cruise interruption by COVID-19, this specific region is important for assessing C_{anth} uptake due to the ventilation of mode water and intermediate water (Gao et al., 2022).

In this work, we present the recent observations along A12 in 2020 and evaluate the changes in DIC and $\delta^{13}C$ from 2010 to 2020. We further apply an extended multiple linear regression (eMLR, Friis et al., 2005) approach to estimate the anthropogenic CO_2 change (ΔC_{anth}) and anthropogenic $\delta^{13}C$ change ($\Delta\delta^{13}C_{anth}$) between 2010 and 2020. The ΔC_{anth} based on $\delta^{13}C$, which is converted using RC values, is also used to compare the two methods for estimating anthropogenic carbon changes. Here, $RC = \Delta\delta^{13}C_{anth}/\Delta C_{anth}$ is the ratio of anthropogenically induced changes in $\delta^{13}C$ and DIC (Ko et al., 2014; McNeil et al., 2001; Quay et al., 2007, 2017). Finally, we investigate the column inventory change (CIC) based on depth-integrated ΔC_{anth} and $\Delta\delta^{13}C_{anth}$.

Our laboratory has developed an analytical method that eventually allows us to simultaneously collect high quality DIC and $\delta^{13}C$ data onboard ship with high spatial resolution. The initial work with a precision of ±0.07‰ for $\delta^{13}C$ was reported previously together with applications to estuarine carbon cycle research (Deng et al., 2022; Su et al., 2019). Due to COVID-19 related restrictions, water samples for this work were taken and analyzed back in the home laboratory. Then, the method was further improved, and samples were collected and analyzed on-board ship for $\delta^{13}C$ during long oceanographic cruises including a 41-day cruise along the North American eastern ocean margin in summer 2022 (Sun et al., 2024) and a 58-day cruise along the GO-SHIP A16N transect in the central and north Atlantic Ocean in spring 2023. This paper represents our first step to use the paired $\delta^{13}C$ and DIC data to constrain C_{anth} storage in the ocean.

2. Materials and Methods

In late austral summer 2020, eight stations (S1–S8) were observed along GO-SHIP A12 line in the southeastern Atlantic Ocean with six stations located north of the subtropical front (STF, Orsi et al., 1995) (Figure 1). The 21 stations (S25–S45 in Figure 1) from the historic A13.5 cruise in 2010 of the Climate and Ocean - Variability, Predictability, and Change (CLIVAR) in the same area (32°–42°S) are used to examine C_{anth} change.

The $\delta^{13}C$ data along A12 in 2020 are measured by our laboratory. And both A12 and A13.5 data sets are now available from Carbon Hydrographic Data Office (CCHDO, https://cchdo.ucsd.edu/).

2.1. Data Collection and Processing

2.1.1. Cruise A12 in 2020

Samples were drawn from Niskin bottles into 60 ml tinted glass vials with septa top covers. Following collection, 0.5 ml sample was withdrawn to create a headspace, 12.5 μL of saturated mercuric chloride solution was added to preserve the sample, and the vial closed using a hard polypropylene cap with Teflon liner. All samples were maintained at the ambient temperature between 16 and 25°C until their return to the University of Delaware laboratory at Newark, DE, where they were processed for $\delta^{13}C$ analysis following the cavity ring-down

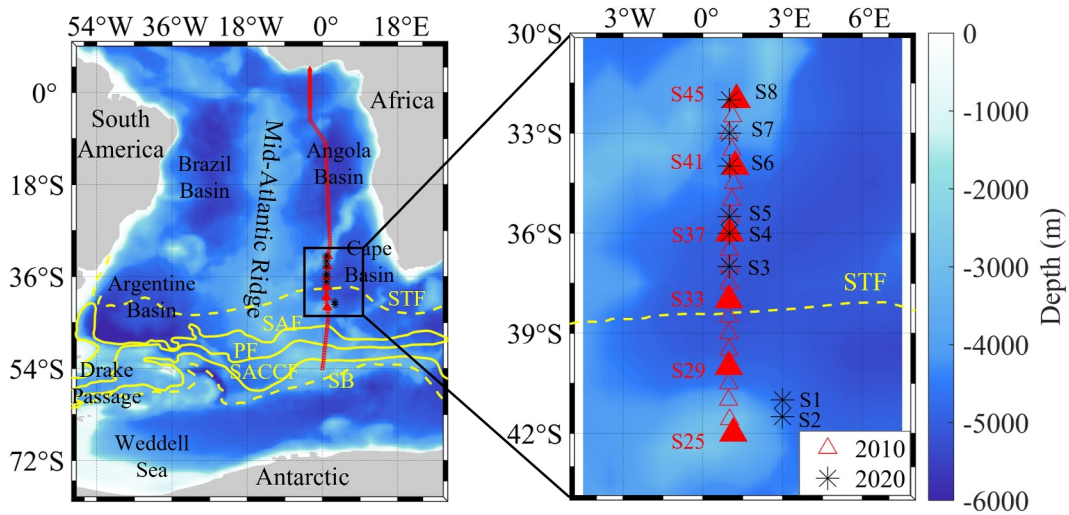

Figure 1. Map of study area and stations. A13.5 stations in 2010 are marked in red triangles among which only red solid triangles with marked numbers include both dissolved inorganic carbon (DIC) and $\delta^{13}C$ measurements. All A12 stations in 2020 are marked in black stars and include both DIC and $\delta^{13}C$ measurements. The yellow lines in the figure represent the ACC fronts. From north to south, these include the subtropical front (STF), subantarctic front (SAF), antarctic polar front (PF), southern ACC front (SACCF), and southern boundary Front (SB).

spectrometer method presented by Su et al. (2019). Briefly, 4 mL of water sample was transferred to and acidified in a CO_2 extraction device, and a CO_2-free air stream was used to purge CO_2 from the water sample. Both ^{12}C and ^{13}C CO_2 signals in the air stream are measured by a Picarro isotope analyzer G2131-I whereas the analytical procedure was controlled and data collected by an analyzer (AS-D1, Apollo Scitech, USA). AS-D1 simultaneously collects both CO_2 concentration and $\delta^{13}C$ data. DIC concentration is determined as the time integrated CO_2 signal whereas $\delta^{13}C$ is the time averaged ^{13}C signal. All analyses were repeated 3–4 times with the mean reported. The $\delta^{13}C$ measurement precision was 0.07‰ (Deng et al., 2022; Su et al., 2019). More recently, the analytical precision has been improved to ±0.03‰ and the procedure has been further automated with a higher efficiency (Sun et al., 2024).

Two $NaHCO_3$ standards of known $\delta^{13}C$ values were used for the $\delta^{13}C$ calibrations. All standards were measured once every 24 hr. Once a week over the duration of analysis, aliquots of standards used in this study were taken in 12 mL vials. At the end of the sample analysis, all standard vials were sent to the UC Davis Stable Isotope Facility for the confirmation of their $\delta^{13}C$ values and corrections to our measured $\delta^{13}C$ were applied. The $\delta^{13}C$ is expressed as $\delta^{13}C\ (‰) = [(DI^{13}C/DI^{12}C)_{sample}/(DI^{13}C/DI^{12}C)_{standard} - 1] \times 10^3$, where the isotopic composition of Peedee belemnite fossil is used as the standard. Phosphate is believed to be correlated with $\delta^{13}C$ in deep water (Broecker & Maier-Reimer, 1992; Claret et al., 2021; Olsen & Ninnemann, 2010). $\delta^{13}C$ data in 2020 is validated based on the relationship between phosphate and $\delta^{13}C$ for deep water (depth ≥2,000 m) in 2010 and 2020 (Text S1 in Supporting Information S1). DIC was measured at sea by the NOAA-AOML group (Wanninkhof et al., 2010). The same group measured DIC in the 2010 cruise with the same method.

$\delta^{13}C$ samples in 2010 and 2020 were analyzed with two different methods in two laboratories. According to the criterion proposed by Quay et al. (2017) and Williams et al. (2021), an offset of +0.07‰ is detected between two $\delta^{13}C$ data sets and an adjustment of +0.07‰ was applied to 2020 $\delta^{13}C$ data to bring them to the same deepwater values (see Text S2 in Supporting Information S1).

2.1.2. Cruise A13.5 in 2010

The water samples were collected in 500 ml glass stoppered bottles. Then, ^{13}C samples are analyzed by isotope mass spectrometer (IRMS) at the National Ocean Sciences AMS lab in Woods Hole. The typical $\delta^{13}C$ measurement precision for these laboratories was ±0.03‰ (Quay et al., 2003).

2.2. The eMLR Approach

The eMLR approach has been widely used to estimate anthropogenic changes in DIC and $\delta^{13}C$ (e.g., Friis et al., 2005; Quay et al., 2017; Sabine et al., 2008). The eMLR approach was developed from the MLR method (Wallace, 1995) to minimize the effects of potential biases in the measured predictors by simultaneously applying the MLRs to data from two cruises. Usually, the MLR equation is built between the observed DIC and $\delta^{13}C$ data with water's physical and biogeochemical properties (e.g., temperature (T), salinity (S), apparent oxygen utilization (AOU), and nutrients (nitrate (N), silicate (Si))) (Brewer, 1978; Chen & Millero, 1979; Quay et al., 2017; Sonnerup et al., 2000; Wallace, 1995). The MLR equations are expressed as follows:

$$X_{t1}{}^{\text{measure}} = a_{t1} + b_{t1} \cdot T_{t1} + c_{t1} \cdot S_{t1} + d_{t1} \cdot \text{AOU}_{t1} + e_{t1} \cdot N_{t1} + f_{t1} \cdot \text{Si}_{t1}$$

$$X_{t2}{}^{\text{measure}} = a_{t2} + b_{t2} \cdot T_{t2} + c_{t2} \cdot S_{t2} + d_{t2} \cdot \text{AOU}_{t2} + e_{t2} \cdot N_{t2} + f_{t1} \cdot \text{Si}_{t2}$$

where X is either DIC or $\delta^{13}C$, a is the intercept, and b, c, d, e, and f are the regression coefficients for each predictive variable, and T, S, AOU, N, and Si are the predictor variables, $t1$ is the earlier cruise, and $t2$ is the later cruise.

To extract anthropogenic changes in DIC and $\delta^{13}C$, the differences between MLR coefficients determined from the earlier and later cruises combined with properties measured at the later time are used. Thus, the eMLR expression of anthropogenic changes in $\delta^{13}C$ and DIC can be written as follows:

$$\Delta X_{\text{anth}}(t_2 - t_1) = (a_{t2} - a_{t1}) + (b_{t2} - b_{t1}) \cdot T_{t2} + (c_{t2} - c_{t1}) \cdot S_{t2} + (d_{t2} - d_{t1}) \cdot \text{AOU}_{t2} + (e_{t2} - e_{t1}) \cdot N_{t2} + (f_{t2} - f_{t1}) \cdot \text{Si}_{t2}$$

It is now customary to use the ensemble eMLR approach with a spatial moving window for constraining anthropogenic carbon based on DIC data following the method of Carter et al. (2017). We do not fully follow this method as the spatial resolution of $\delta^{13}C$ data is not as high as DIC. We applied the eMLR method to each characterized water masses based on neutral density (γ): 1. Surface Water (SW) with $\gamma < 26.80$ kg m^{-3}; 2. Subantarctic Mode Water (SAMW) with $26.80 < \gamma < 27.23$ kg m^{-3}; 3. Antarctic Intermediate Water (AAIW) with $27.23 < \gamma < 27.5$ kg m^{-3}; 4. Upper Circumpolar Deep Water (UCDW) with $27.5 < \gamma < 28$; 5 kg m^{-3}; and Lower Circumpolar Deep Water (LCDW) and Antarctic Bottom Water (AABW) with $\gamma > 28$ kg m^{-3}. We combined the last two water masses into one (Gao et al., 2022). We also incorporate some modifications of the ensemble eMLR into our approach, that is, we use "robust" regression instead of "stepwise" regression. Coefficients for MLR equations and statistical significances are shown in Tables S1–S4 in Supporting Information S1.

2.3. Anthropogenic CO_2 and $\delta^{13}C$ Change Estimation in the Mixed Layer

Since the upper mixed layer waters are strongly affected by seasonal physical and biological processes and the exchange rate of CO_2 between seawater and atmospheric is relatively slow (DIC equilibration time is upper to 1 year, Broecker & Peng, 1974), the MLR and eMLR approaches are not suitable for DIC to be applied to the upper mixed layer waters (Sabine et al., 2008). The mean mixed layer depth is about 50 m in the study region. For water masses in the upper 50 m, we used the constant pCO_2 difference approach between 2010 and 2020 to estimate ΔC_{anth}, which assuming the sea surface pCO_2 increase follows the atmospheric increase (Carter et al., 2017; Gao et al., 2022). Additionally, we verified that in the study region, the decadal rate of sea surface pCO_2 increase is comparable to the rate of atmospheric CO_2 increase (Figure S4, Table S6 in Supporting Information S1). Alternatively, one could extend the eMLR equations from below 50 m into the top 50 m water (Gruber, Clement, et al., 2019).

For $\delta^{13}C$, we took three approaches. First, we followed a similar transient equilibrium approach that is applied to DIC (McNeil et al., 2003), assuming the sea-surface $\delta^{13}C$ follows the change in the atmosphere. In other words, this approach involves calculating $\Delta\delta^{13}C_{\text{anth}}$ as the difference in air-sea equilibrated $\delta^{13}C$ between two survey periods. Second, similar to the previous DIC-based approach, we also extended the eMLR equations from depths below the 50 m into the top 50 m water column. Third, we explored the applicability of the eMLR method for $\delta^{13}C$ to the entire upper mixed layer.

Here, we detailed the calculation steps of the transient equilibrium approach. (a) We extracted acceptable data (quality flag = 2 or 6) from each cruise. (b) Given the nonidentical locations of the two cruises, we interpolated the water properties from the first cruise to match the location of each data point in the second cruise using the inverse distance weighting (IDW) scheme. (c) We calculated the DIC species distribution in equilibration with the atmosphere in each cruise using CO2SYS for Matlab (van Heuven et al., 2011) based on the corresponding atmospheric CO_2 value at the time of the cruise and the alkalinity measured in this cruise as well as other properties, such as salinity, temperature, pressure, silicate, and phosphate. Then, the $\delta^{13}C$ of surface seawater DIC in equilibrium with the atmosphere is derived from weighted sum of the equilibrium fractionation factors between gaseous CO_2 and two dominant DIC species (HCO_3^- and CO_3^{2-}) (Zhang et al., 1995). (d) The difference in air-sea equilibrated $\delta^{13}C$ between the two cruises was designated as $\Delta\delta^{13}C_{anth}$.

3. Results and Discussion

3.1. Decadal Changes of DIC and $\delta^{13}C$ From 2010 to 2020

Data from eight stations were collected in late austral summer of 2020 along transect A13.5 in the southeastern Atlantic Ocean with six stations (S3–S8) located north of the STF and two stations (S1 and S2) located south of this front (Figure 1). Due to COVID-19 restrictions, this cruise was terminated after one week of work with its coverage reduced to a narrow band from 42°S to 32°S, and it was subsequently renamed A12. However, this latitude band features substantial C_{anth} absorption and is an important area for mode and intermediate water ventilation (Gao et al., 2022). To our knowledge, this is also the only observation-based estimate of oceanic C_{anth} accumulation rate in the most recent decade despite the data limitation.

At the sea surface, $\delta^{13}C$ increases from north to south (Figure 2). This meridional $\delta^{13}C$ trend is largely dictated by the isotopic fractionation between CO_2 gas and ocean DIC, which depends strongly on temperature. The equilibrium fraction factor increases with decreasing ocean surface temperature (~−0.12‰/°C) (Charles et al., 1993; Mook et al., 1974). Using the equilibrium fractionation equation, we estimated an equilibrated $\delta^{13}C$ being more negative (−0.23‰) in warm subtropical waters (21.68°C) and more positive (0.63‰) in cold subpolar waters (13.29°C) (Zhang et al., 1995). The equilibrium fractionation difference between the warm and cold waters (0.86‰) is slightly larger than the observation-based difference (0.77‰), indicating other processes, possibly stronger biological production, also contribute to a more positive $\delta^{13}C$ in the southern waters (Figure S6 in Supporting Information S1). Alternatively, there may be insufficient time for the full equilibrium of $^{13}CO_2$ between the atmosphere and the surface ocean in the subpolar waters (Broecker & Maier-Reimer, 1992; McNeil et al., 2001).

Vertically, the preferential uptake of ^{12}C over ^{13}C into the biomass during biological production increases the $\delta^{13}C$ of the mixed layer, while remineralization of this biological carbon at depth reverses the process. These effects can obscure an assessment of transient changes in $\delta^{13}C$ related to the oceanic ^{13}C Suess effect. In the SW and SAMW, DIC increases while $\delta^{13}C$ generally decreases from the surface to the deep depths. Below the SAMW, DIC remains relatively high and $\delta^{13}C$ is low in the UCDW, LCDW, and AABW. Slightly higher $\delta^{13}C$ value of 0.8–1.1‰ between approximately 600 and 1,200 m depth correlates well with the depth of the core of AAIW, which brings newly subducted water and progressively deepens to the north in this region across these latitudes. Underneath the AAIW, DIC maximum and $\delta^{13}C$ minimum are observed at about 1,500 m, corresponding to the core of the UCDW characterized by an oxygen minimum zone (O_2 < 200 μmol kg^{-1}, Figure S5 in Supporting Information S1). Between the UCDW and LCDW, a source water mass originates from North Atlantic, that is, a remnant core of NADW is still recognizable by the deeper salinity maximum (Figure S5 in Supporting Information S1), characterized by a local DIC minimum and $\delta^{13}C$ maximum centered at about 2,500 m. Additionally, this core of minimum DIC (maximum $\delta^{13}C$) shoals toward the south. Waters in the bottom layer (LCDW and AABW) exhibit relatively high DIC and low $\delta^{13}C$.

Due to the spatial limitation to the narrow band and relatively high analytical uncertainty (±0.07‰) in the 2020 study, we aggregated all stations in the study area to achieve our primary objective of assessing C_{anth} in this region, disregarding potential subregional variations. The vertical profiles of all measured DIC data and their horizontal mean are very similar in 2010 and 2020 (Figure 3a). The mean DIC in 2020 is higher than 2010 at different depths, suggesting inputs from C_{anth}. The DIC difference (ΔDIC, measured DIC in 2020 minus that in 2010) in the upper 50 m layer is only 4.65 ± 5.13 μmol kg^{-1}, which is less than the atmospheric equilibrated value (11.4 μmol kg^{-1}). Although the DIC increase in the subsurface 50–200 m layer (11.99 ± 9.34 μmol kg^{-1}) (Figure

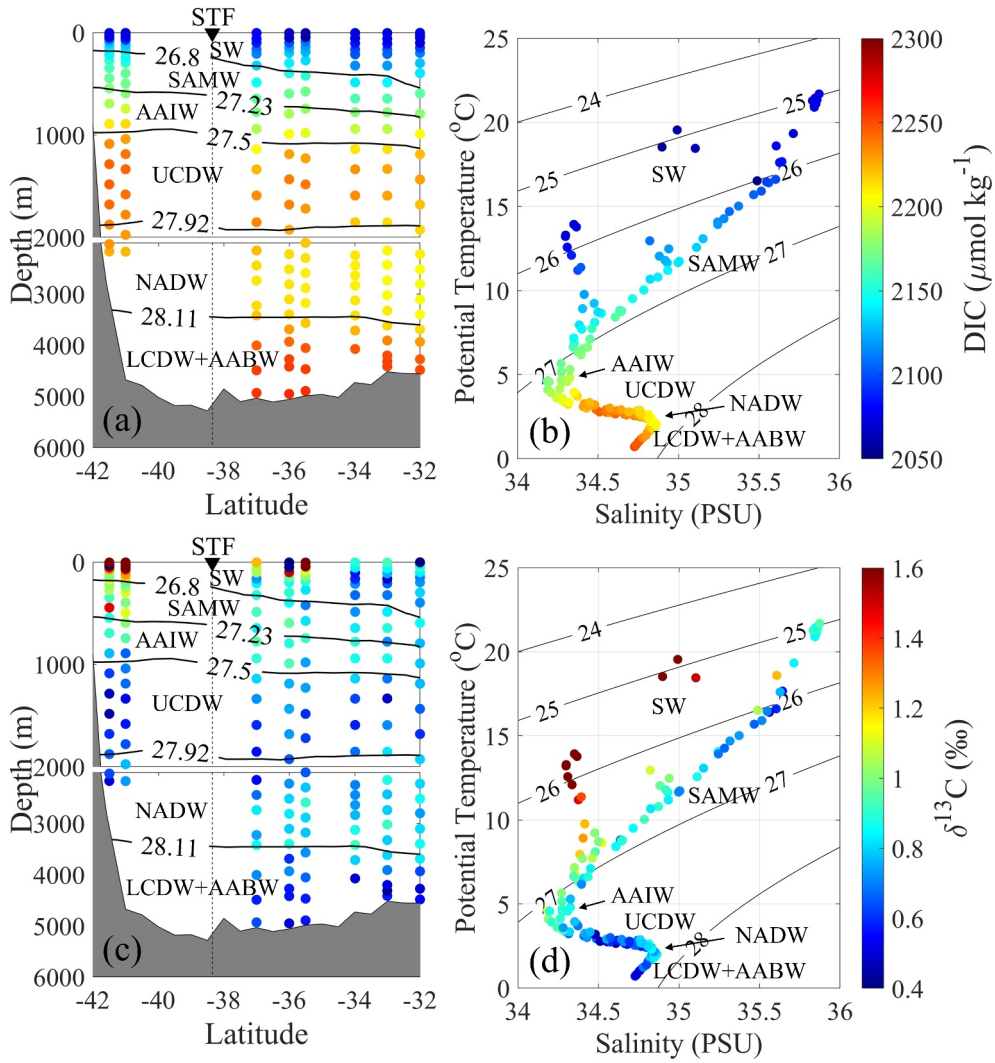

Figure 2. Vertical distribution of (a) dissolved inorganic carbon (DIC) and (c) $\delta^{13}C$ at each station along transect A12 occupied in 2020 and *T-S* plot of (b) DIC and (d) $\delta^{13}C$ along A12 2020. Acronyms in the figure are subtropical front (STF) and water masses: Surface Water (SW), Subantarctic Mode Water (SAMW), Antarctic Intermediate Water (AAIW), Upper Circumpolar Deep Water (UCDW), North Atlantic Deep Water (NADW), Lower Circumpolar Deep Water (LCDW), and Antarctic Bottom Water (AABW).

S4 in Supporting Information S1) closely matches that predicted from the atmospheric CO_2 increase. The less than expected DIC increase in surface water is attributed to the different seasonal variations in the two data sets collected a decade apart. We made this attribution as the long-term sea surface pCO_2 tracks the atmospheric pCO_2 well (Figure S4 in Supporting Information S1). From 400 to 2,000 m, ΔDIC shows an exponential decrease and remains nearly constant below 2,000 m, reflecting waning temporal DIC changes with depth. Comparably, the distribution of DIC in various water masses demonstrates the decline in ΔDIC from the surface layer to bottom layer (Figure 3c).

$\delta^{13}C$ provides an alternative way for assessing C_{anth} accumulation in the ocean (i.e., Quay et al., 1992). Similar to the decadal DIC increase (Figure 3a), $\delta^{13}C$ notably decreased between the two cruises (black stars and red triangles in Figure 3b) especially in the subsurface water. From 2010 to 2020, the atmospheric $\delta^{13}C$ decreased from −8.38‰ to −8.63‰ (based on https://cdiac.ess-dive.lbl.gov), and the average sea surface $\delta^{13}C$ in the study region decreased from 1.65 ± 0.16‰ to 1.36 ± 0.39‰. The mean temporal changing rate of $\Delta\delta^{13}C$ (-0.24 ± 0.18‰ decade^{-1}) in the surface layer (~10 m) is similar to that in the atmospheric (−0.25‰ decade^{-1}). The contrast between the tracking of water $\delta^{13}C$ with the atmospheric $\delta^{13}C$ and a seemingly decoupled water DIC

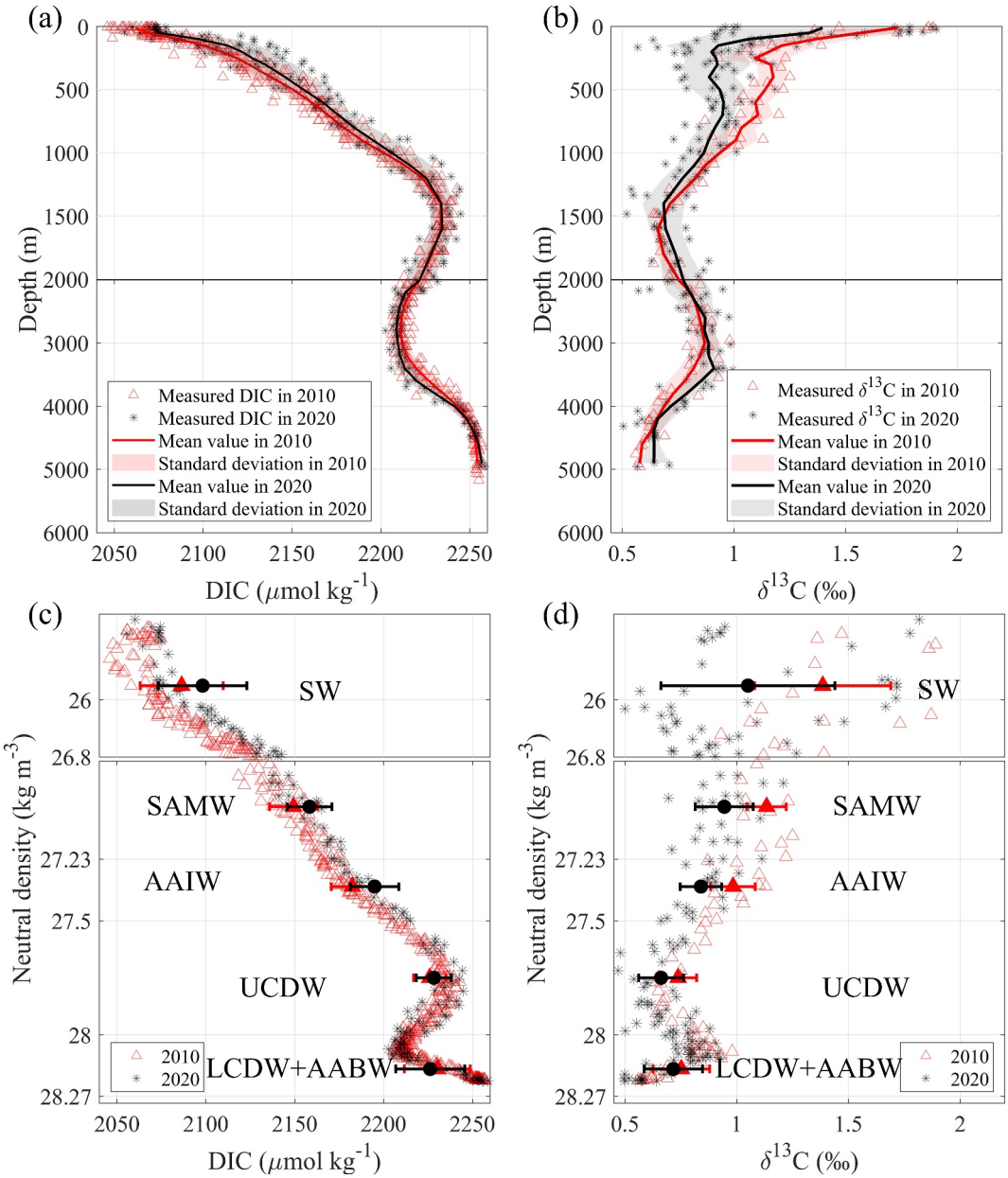

Figure 3. Vertical profiles of (a) dissolved inorganic carbon (DIC) and (b) δ^{13}C measured in 2010 and 2020 in the region of 1°–3°E and 32°–42°S. Panels (c) and (d) are similar to (a) and (b) but vertically averaged within five characteristic water mass layers.

with the atmospheric pCO_2 can be explained by the fact that the isotopic equilibration time for δ^{13}C is ~10 years and is more than 10 times longer than that for DIC and CO_2. In other words, δ^{13}C data are less affected by seasonal or even interannual variations and reflect more on longer time changes. Such a decadal δ^{13}C change rate can be quantified by analytical instruments with high confidence. Thus, δ^{13}C exhibits a higher signal-to-noise ratio than DIC (Figure 3b vs. Figure 3a; Figure 3d vs. Figure 3c). In the surface layer of the study region, the relative changes of δ^{13}C (about 18%) are much higher than that of DIC (0.5%) over the 10-year period. Vertically, the ratio of the maximum rate of decadal increase in DIC (about 11 μmol kg^{-1} decade^{-1}) to the vertical increase from the surface to 1,000 m (about 135 μmol kg^{-1}) is only 0.08 decade^{-1}. In contrast, the maximum rate of decadal change in δ^{13}C is −0.3‰ decade^{-1} whereas the vertical decrease from surface to 1,000 m is −0.8‰, resulting in a greater

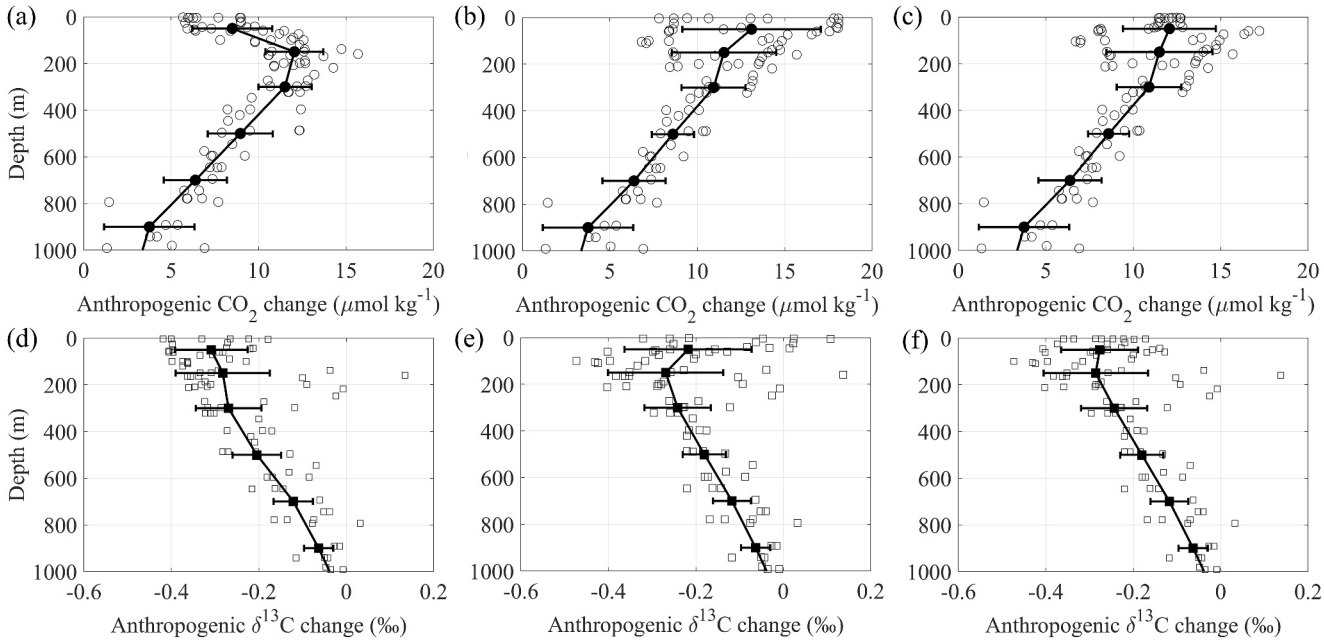

Figure 4. Anthropogenic CO_2 and $\delta^{13}C$ change in the upper 1,000 m layer. Panels (a) and (d) anthropogenic CO_2 and $\delta^{13}C$ change estimated by the extended multiple linear regression (eMLR) method with all the acceptable samples, (b) and (e) anthropogenic CO_2 and $\delta^{13}C$ change estimated by the eMLR method without samples in the top 50 m layer, and then the eMLR equation is extended into the surface 50 m, (c) and (f) anthropogenic CO_2 and $\delta^{13}C$ change estimated by the eMLR method below 50 m combined with anthropogenic CO_2 and $\delta^{13}C$ change estimated by the constant pCO_2 difference approach (Carter et al., 2017) and the transient equilibrium approach (McNeil et al., 2003) separately in the 50 m layer. Note: Panel (c) is identical to the black circles in Figure 5a, and panel (d) is identical to Figure 5b, but only the upper 1,000 m layer is displayed.

ratio of 0.38 decade^{-1}. Moreover, this high signal-to-noise ratio can be verified from the perspective of water masses (Figures 3c and 3d).

Our results here support the proposition made by Quay and coworkers that $\delta^{13}C$ could be a more sensitive tracer than DIC for quantifying C_{anth} invasion in the ocean due to its stronger anthropogenic perturbation than natural variability in space and time (Körtzinger et al., 2003; Quay et al., 2003, 2007, 2017; Sonnerup & Quay, 2012). Quay also argued this perspective from the standpoint of analytical method sensitivity (Quay et al., 2003, 2007). Nevertheless, we propose that employing a combination of both DIC concentration and stable isotope signals is the preferred approach moving forward. These reasons motivate us to investigate the direct comparison between the ΔC_{anth} and $\Delta\delta^{13}C_{anth}$ in the next two sections.

3.2. Exploration of Methods Estimating Anthropogenic $\delta^{13}C$ Changes in the Upper Mixed Layer

There is considerable uncertainty for DIC in applying the eMLR method to detect anthropogenic signal change within the upper mixed layer, largely due to strong seasonal variability affected by physical and biological processes. However, considering that the air-sea equilibrium time for $\delta^{13}C$ is 10 times that of DIC, seasonal changes impact $\delta^{13}C$ to a much lesser extent about one tenth compared to DIC. Thus, we suggest that $\delta^{13}C$ may have an advantage over DIC in applying eMLR to estimate anthropogenic carbon changes in the upper mixed layer. To test this hypothesis, we conducted some sensitivity tests for ΔC_{anth} and $\Delta\delta^{13}C_{anth}$ the upper mixed layer (Figure 4). Since the mean mixed layer depth is 49.5 m from March to April in the study region, which is calculated from the mixed layer climatology of Holte et al. (2017), we focused on the different treatments for the upper 50 m:

1. constructing eMLR equations using all the acceptable samples to estimate ΔC_{anth} and $\Delta\delta^{13}C_{anth}$ for each corresponding water mass (Figures 4a and 4d).
2. constructing eMLR equations to estimate ΔC_{anth} and $\Delta\delta^{13}C_{anth}$ below 50 m and then extending the eMLR equations in the SW into the top 50 m water (Figures 4b and 4e).

3. estimating ΔC_{anth} and $\Delta\delta^{13}C_{anth}$ in the upper 50 m based on the assumption that the CO_2 and the isotope ratio in the surface layer follow the changes in atmospheric CO_2 on decadal timescale (Figures 4c and 4f).

When including the upper 50 m to establish the eMLR equations (the first treatment), the estimated ΔC_{anth} based on DIC is lower in the surface than that in the subsurface below 50 m (Figure 4a), which is unreasonable. The trend of ΔC_{anth} estimated by the first treatment differs noticeably from the trend of ΔC_{anth} estimated by the second and third treatments (Figure 4a vs. Figures 4b and 4d). Specifically, ΔC_{anth} in the upper 50 m layer estimated by the third treatment averages around 12 μmol kg^{-1} (Figure 4c). Although ΔC_{anth} estimated by the first treatment increases from only 5 μmol kg^{-1} at the surface to 15 μmol kg^{-1} at a depth of 50 m, then decreases with increasing depth. In contrast, the results from all three approaches remain quite reasonable for $\delta^{13}C$ based analyses. $\Delta\delta^{13}C_{anth}$ is relatively consistent with depth when using the first treatment (Figure 4d). The trend of $\Delta\delta^{13}C_{anth}$ estimated by the first treatment is mirrored by that of ΔC_{anth} estimated by the second and third treatment (Figure 4d vs. Figures 4b and 4d). Moreover, $\Delta\delta^{13}C_{anth}$ estimated by the third treatment clusters around 3‰ (Figure 4f), which is comparable to that estimated by the first treatment (Figure 4d). Furthermore, the trend of ΔC_{anth} estimated by the third treatment shows a close relationship to $\Delta\delta^{13}C_{anth}$ estimated by the first and third treatments (Figure 4c vs. Figures 4d and 4f).

Thus, estimation of ΔC_{anth} in the mixed layer using the eMLR method has a large and unacceptable uncertainty, whereas the uncertainty is reduced for $\delta^{13}C$. This can be attributed mostly to the fact that $\delta^{13}C$ data are integrated over an interannual timescale, meaning that season variations, thermal cycles, and biological changes have minimal effect on its distribution. In contrast, the characteristic air-sea exchange time for CO_2 in the mixed layer is less than 1 year (Broecker & Peng, 1974). Given that the air-sea equilibration times for $^{13}CO_2$ are 10 times longer than those for $^{12}CO_2$, $\delta^{13}C$ exhibits greater air-sea disequilibrium compared to DIC. Therefore, it is more appropriate to apply eMLR to $\delta^{13}C$ than DIC data to estimate anthropogenic carbon changes in the upper mixed layer.

However, the applicability of the eMLR also depends on the stability of the relationship between the carbon tracer and the set of predictors used, such as the limitations associated with using oxygen/AOU as a predictor in the upper mixed layer (with a short equilibrium timescale of approximately 1 month). Thus, this approach has its constraints. Nevertheless, given the absence of a universally accepted best approach for estimating anthropogenic carbon changes in the mixed layer, we contend that further methodological investigations are required. This section demonstrates our exploration. In addition, regarding the limitations of using oxygen/AOU as an independent variable, it may be necessary to introduce an adjustment to AOU or DIC/$\delta^{13}C$ to mitigate potential additional changes in biogeochemical DIC cycling (e.g., adjustments based on AOU changes (Carter et al., 2017; Sabine et al., 2008) or utilizing C*/δ^{13}C* or C^/δ^{13}C^ instead of DIC/$\delta^{13}C$ (Carter et al., 2019; Clement & Gruber, 2018; Gruber, Clement, et al., 2019; Müller et al., 2023). Given the limitations of this study, further exploration will be left to future work.

3.3. Estimate of Anthropogenic CO_2 and $\delta^{13}C$ Changes

Though all three approaches are employed to assess ΔC_{anth} and $\Delta\delta^{13}C_{anth}$ in the upper mixed layer (Section 3.2) for ΔC_{anth} (based on DIC data), we only present the one from eMLR below 50 m depth and tracking atmospheric pCO_2 in surface water based on the community consensus (Carter et al., 2017, 2019; Clement & Gruber, 2018; Gruber, Clement, et al., 2019; Müller et al., 2023). However, for $\Delta\delta^{13}C_{anth}$, since both the eMLR method and transient equilibrium approach yielded similar values, and the eMLR method involves no additional assumption, we present the eMLR result here. This is also consistent with the approach made by previous literature (Olsen et al., 2006; Quay et al., 2017; Racapé et al., 2013; Williams et al., 2021), and thus the result can be better comparable.

The estimates of both ΔC_{anth} and $\Delta\delta^{13}C_{anth}$ (Figures 5a and 5b) show strong signals in the upper 1,000 m. The strongest ΔC_{anth} of more than 10 μmol kg^{-1} occurs in the upper 200 m depth layer (Figure 5a), whereas the strongest $\Delta\delta^{13}C_{anth}$ signal, with a mean value of up to -0.31 ± 0.08‰, is found within the upper 100 m of the water column (Figure 5b). This difference may partly reflect the different timescales of the two tracers and the methodological considerations. When averaged within the density boundaries of characteristic water masses (Figures 5c and 5d), significant ΔC_{anth} and $\Delta\delta^{13}C_{anth}$ can be visible within the SW ($\Delta C_{anth} = 10.93 \pm 1.45$ μmol kg^{-1}; $\Delta\delta^{13}C_{anth} \sim = -0.30 \pm 0.06$‰; spatial mean ± spatial standard deviation) and SAMW ($\Delta C_{anth} = 8.11 \pm 2.11$ μmol kg^{-1}; $\Delta\delta^{13}C_{anth} = -0.16 \pm 0.05$‰). Relatively larger ΔC_{anth} and $\Delta\delta^{13}C_{anth}$ are also observed in the AAIW

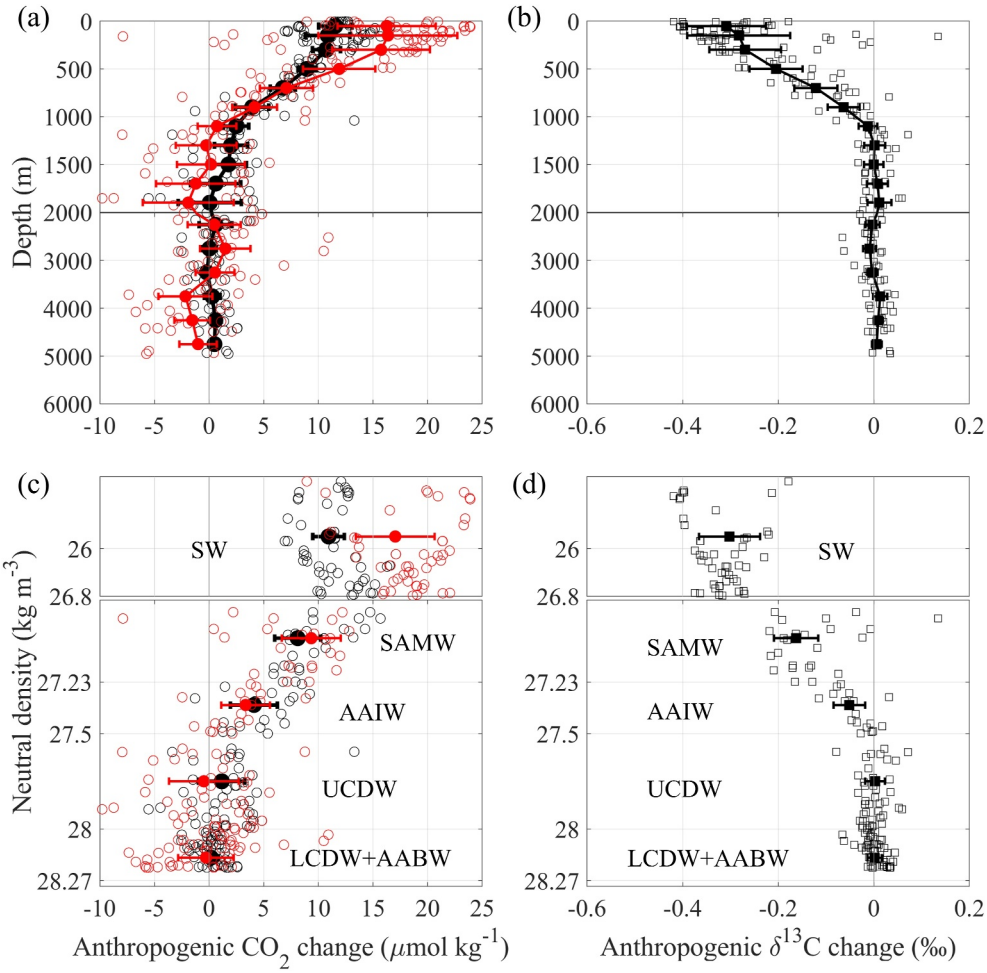

Figure 5. Depth profile of (a) anthropogenic CO_2 change estimated by dissolved inorganic carbon (DIC, black) and $\delta^{13}C$ using RC values (red), (b) anthropogenic $\delta^{13}C$ change between 2010 and 2020. Panels (c) and (d) are similar to (a) and (b) but vertically averaged within five characteristic water mass layers.

($\Delta C_{anth} = 4.11 \pm 2.15$ μmol kg^{-1}; $\Delta\delta^{13}C_{anth} = -0.05 \pm 0.03$‰). Small anthropogenic change signals can be found in the water masses below AAIW (UCDW: $\Delta C_{anth} = 1.16 \pm 2.12$ μmol kg^{-1}; $\Delta\delta^{13}C_{anth} = 0.003 \pm 0.02$‰; LCDW and AABW: $\Delta C_{anth} = 0.17 \pm 0.66$ μmol kg^{-1}; $\Delta\delta^{13}C_{anth} = 0.002 \pm 0.02$‰). The uncertainties from measurement inaccuracies of fit parameters can be assessed through Monte Carlo simulation, which randomly perturbs the data sets with a noise (Carter et al., 2017; Hauck et al., 2010; Tanhua et al., 2007; Ulfsbo et al., 2018). Following Carter et al. (2017), we performed the Monte Carlo simulation 10,000 times with the parameters DIC, $\delta^{13}C$, T, S, AOU, N, and Si with perturbations of 2, 0.07, 0.002, 0.002, 2, 0.4, and 0.4, respectively. The resulting total mean errors for ΔC_{anth} and $\Delta\delta^{13}C_{anth}$ in the water masses SW, SAMW, AAIW, UCDW, LCDW, and AABW are -0.13 ± 0.44, 0.02 ± 0.61, 0.94 ± 1.02, -0.53 ± 0.40, and -0.86 ± 0.40 μmol kg^{-1} and 0.02 ± 0.02, -0.002 ± 0.05, -0.002 ± 0.07, 0.001 ± 0.03, and 0.008 ± 0.02‰ respectively. The more recent water mass (i.e., SW) has a greater $\delta^{13}C_{anth}$ decrease and C_{anth} increase signal due to its active exchange with the contemporary atmosphere compared to older water masses (Figure 5, i.e., AAIW is older than SAMW, and SAMW is older than the SW). The older denser water masses remain more isolated from the atmosphere and thus influenced by historical atmospheric conditions.

In order to directly compare the estimated anthropogenic carbon changes by the two methods, $\Delta\delta^{13}C_{anth}$ is converted to ΔC_{anth} (red circles in Figures 5a and 5c) using RC values. We use RC values from literature (RC values calculated from our own ΔC_{anth} and $\Delta\delta^{13}C_{anth}$ estimations along A13.5 are discussed in Section 3.4). The

RC value for the upper 50 m is set to −0.020‰ (μmol kg^{-1})$^{-1}$ based on the decade-long $\delta^{13}C$ and DIC time series measurements at the Drake Passage (−0.021‰ (μmol kg^{-1})$^{-1}$) and Hawaii Ocean Time-series (−0.018‰ (μmol kg^{-1})$^{-1}$) with a two to one ratio in weight (Quay et al., 2017). The RC values below 50 m are derived from Eide et al. (2017). The two estimates of ΔC_{anth} agree quite well below 500 m. In the upper 500 m, both estimates show the strongest ΔC_{anth} signal of the water column, but the estimate by $\delta^{13}C$ methods (15.45 ± 6.51 μmol kg^{-1} decade^{-1}) is 26% ($p < 0.01$) larger than that by the DIC method (11.44 ± 2.59 μmol kg^{-1} decade^{-1}) (Figure 5a). For the characteristic water masses, the ΔC_{anth} estimates by $\delta^{13}C$ are much larger than that by DIC only in SW (Figure 5c) but very close to each other in the other deeper water masses (SAMW, AAIW, UCDW, LCDW, and AABW), where the DIC are less affected by seasonal variations and isolated from the atmosphere. This indicates that the two methods are actually comparable in estimating ΔC_{anth} in all of the old-age mode and intermediate water masses below SW. Where the ventilation age of mode and intermediate water is approximately several years to several decades, whereas the age of SW is approximately several years (Figure S7 in Supporting Information S1).

It is not surprising that high ΔC_{anth} centered at the upper ocean layer, especially in the SW, SAMW, and AAIW. This is because C_{anth} primarily comes from the air-sea exchange. In addition, the formation of mode and intermediate water masses and the consequent ocean ventilation have important roles in convection of the C_{anth} stored in the upper waters toward the inner ocean (Gao et al., 2022; Müller et al., 2023; Sallée et al., 2012). In the South Atlantic Ocean, SAMW is originated in the north and AAIW in the south of SAF originated near the Drake Passage and advected eastward into the eastern basin (Talley, 2011). Although subduction of SAMW and AAIW is weaker in the eastern basin than the western basin, the water mass in the study region is also influenced by contributions from the Indian Ocean through Agulhas rings, eddies, and filaments, a phenomenon known as Agulhas leakage (Biastoch et al., 2008). Agulhas eddies are capable of taking up more CO_2 from the atmosphere than their surrounding waters (Orselli et al., 2019), and the structures of anticyclonic Agulhas eddies are also in favor of the C_{anth} penetration.

3.4. RC Values

In the literature, RC values are commonly utilized to estimate the C_{anth} uptake rate from $\Delta\delta^{13}C_{anth}$ (e.g., Ko et al., 2014; McNeil et al., 2001; Quay et al., 2007, 2017). The magnitude of RC depends on the air-sea CO_2 gas exchange rate and exposure time of the surface waters before subduction (McNeil et al., 2001). Because the air-sea equilibration time for $\delta^{13}C$, at ∼10 years, is 10 times longer than for CO_2, a water parcel that remains at the surface for a longer time will obtain greater $\delta^{13}C$ equilibration and have a higher RC value. RC values can be calculated directly by $\Delta\delta^{13}C_{anth}$ and ΔC_{anth} (McNeil et al., 2001; Quay et al., 2017) and by the ratio of preformed DIC (DIC^0) and $\delta^{13}C_{DIC}$ ($\delta^{13}C^0$) (Ko & Quay, 2020; Körtzinger et al., 2003; Quay et al., 2007).

As shown in Section 3.3, we estimated the ΔC_{anth} and $\Delta\delta^{13}C_{anth}$ in each water mass, yielding the mean RC values of −0.0280, −0.0136, and −0.0087‰ (μmol kg^{-1})$^{-1}$, respectively, for SW, SAMW, and AAIW. The mean RC value is −0.0233 ± 0.0153‰ (μmol kg^{-1})$^{-1}$ according to the eMLR-based estimates of $\Delta\delta^{13}C_{anth}$ and ΔC_{anth} for the water masses below 50 m and within the neutral density (γ) of 26.8–27.5 kg m^{-3}, that is, SW, SAMW, and AAIW. This value is similar to that reported (−0.024 ± 0.003‰ (μmol kg^{-1})$^{-1}$) in the North Atlantic Ocean (Körtzinger et al., 2003) and agrees well with estimates in the Pacific Ocean (Quay et al., 2017) but considerably larger than that estimated in the Southern Ocean (0.007−0.015‰ (μmol kg^{-1})$^{-1}$) for 42°−54°S (McNeil et al., 2001).

Eide et al. (2017) have provided RC for the global ocean, including the South Atlantic Ocean. Their values are −0.017 ± 0.003, −0.018 ± 0.003, −0.013 ± 0.002, and −0.009 ± 0.002‰ (μmol kg^{-1})$^{-1}$, respectively, for the isopycnals of σ_θ = 26.8, 27.0, 27.2, and 27.4 kg m^{-3}. Utilizing these RC values, we observed that the depth profile of ΔC_{anth} based on DIC and $\delta^{13}C$ shows good consistency except for depths shallower than 100 m and deeper than 4,000 m (Figure 5a). Notably, for the characteristic water mass layer, only ΔC_{anth} in the SW estimated by $\Delta\delta^{13}C_{anth}$ and RC are significantly higher than that estimated by DIC. This discrepancy may partly arise from RC values of −0.020 and −0.017‰ (μmol kg^{-1})$^{-1}$ applied to water masses shallowing 50 m and the SW, which are less negative than our estimated RC value for SW (−0.028‰ (μmol kg^{-1})$^{-1}$) via ΔC_{anth} and $\Delta\delta^{13}C_{anth}$. ΔC_{anth} in the other water masses derived from $\Delta\delta^{13}C_{anth}$ and RC is slightly lower than that estimated based on DIC (Figure 5c). Overall, ΔC_{anth} values estimated based on both DIC and $\delta^{13}C$ generally fall within the uncertainty range of the average value except for the SW.

Table 1
Depth-Integrated Changes in $\delta^{13}C$ and Dissolved Inorganic Carbon (DIC) in the Upper 2,000 m During 2010–2020 at Each Station

Station no.	Depth-integrated $\delta^{13}C$ change, ‰ m yr^{-1} (offset corrected)	CIC by $\delta^{13}C$/RC, mol m^{-2} yr^{-1}	CIC by DIC, mol m^{-2} yr^{-1}
1 (3.00°E, 41.00°S)	−11.75	0.92	1.45
2 (3.00°E, 41.50°S)	−12.46	0.95	1.29
3 (1.00°E, 37.00°S)	−24.69	1.57	1.15
4 (0.99°E, 36.00°S)	−15.11	0.84	1.20
5 (1.00°E, 35.50°S)	−16.32	0.90	1.09
6 (1.01°E, 33.99°S)	−23.02	1.18	0.77
7 (1.00°E, 33.00°S)	−19.00	0.80	0.66
8 (1°E, 32.00°S)	−18.43	0.80	0.57
Mean ± standard deviation	−17.60 ± 4.64	1.00 ± 0.26	1.02 ± 0.32

The RC value varies depending on location and water mass ages (Eide et al., 2017; Ko et al., 2014; Körtzinger et al., 2003; McNeil et al., 2001). Variations in RC values are also caused by the selection of density and age of distinct water masses. Further exploration of RC values is necessary, particularly regarding the relationships between $\delta^{13}C^0$ and DIC^0 or the ratio of $\Delta\delta^{13}C_{anth}$ to ΔC_{anth}. Naturally, getting the RC value correct is essential to converting $\Delta\delta^{13}C_{anth}$ to ΔC_{anth}. As a result, even though ^{13}C has a greater signal-to-noise ratio, the necessity of using the RC value introduces more uncertainty, making RC uncertainty estimations crucial.

3.5. Anthropogenic CO_2 Uptake Rates Based on Column Inventory Changes

The depth-integrated $\delta^{13}C$ change is a measure of the total amount of $\delta^{13}C_{anth}$ accumulation in the water column (Quay et al., 1992). Assuming that $\Delta\delta^{13}C_{anth}$ is negligible below 2,000 m (Quay et al., 2017), the depth integration from the sea surface to 2,000 m is used in this study. The depth-integrated $\delta^{13}C$ change in the upper 2,000 m at each station ranges from −24.46 to −11.75‰ m yr^{-1} with a spatial mean and standard deviation of −17.60 ± 4.64‰ m yr^{-1} for our study region (Table 1). This rate is similar to that reported for 40°S in the Indian Ocean (−18.4 ± 7.8‰ m yr^{-1}) with the integration depth of 1,400 m from 1978 to 1995 (Sonnerup et al., 2000) but slightly higher than −14‰ m yr^{-1} for a similar latitude band in the eastern South Pacific Ocean with an integration depth of 200–1,500 m from 1994 to 2008 (Ko et al., 2014). The similar rates around this latitudinal band of Southern Ocean mode water formation indicate strong C_{anth} absorption from $\delta^{13}C$ signals compared to the subtropical band at lower latitudes (Ko et al., 2014).

Anthropogenic CO_2 uptake rates along a transect or in an ocean basin are often measured by CIC, that is, depth-integrated CO_2 change (e.g., Sabine et al., 2004) and depth-integrated $\delta^{13}C$ change divided by RC ($\Delta\delta^{13}C_{anth}$/RC, e.g., Quay et al., 2007). In the study region, the CIC based on DIC ranges from 0.57 mol m^{-2} yr^{-1} in the north to 1.45 mol m^{-2} yr^{-1} in the south (Table 1) with a spatial mean and standard deviation of 1.02 ± 0.32 mol m^{-2} yr^{-1}. Meanwhile, the CIC by $\Delta\delta^{13}C_{anth}$/RC ranges from 0.80 to 1.57 mol m^{-2} yr^{-1} with a spatial mean and standard deviation of 1.00 ± 0.26 mol m^{-2} yr^{-1}. Thus, both DIC-based and $\delta^{13}C$-based CIC values reveal similar C_{anth} uptake from 2010 to 2020. Note that if we did not correct the $\delta^{13}C$ of the 2020 and force it to equal to the 2010 $\delta^{13}C$ below 2,000 m, the CIC based on $\delta^{13}C$ would be greater. On the whole, CIC values based on $\delta^{13}C$ and DIC are quite close despite their distinct latitudinal distributions.

Transect A13.5 was first observed in 1983/84, and the ΔC_{anth} along A13.5 between 1983/84 and 2010 has been studied by our previous work (Gao et al., 2022). To have a direct comparison with the historical CIC rate, ΔC_{anth} based on DIC in this study is gridded on a 0.5° by 50 m with an IDW scheme. Using this approach, the CIC is 1.08 ± 0.26 mol m^{-2} yr^{-1} from 2010 to 2020, representing an increased rate compared to 0.87 ± 0.05 mol m^{-2} yr^{-1} from 1983/84 to 2010 at the same location. This increase is statistically significant, as the *t*-test of these two CIC rates rejects the null hypothesis at the 5% significance level ($p < 0.05$). Thus, CIC during 2010–2020 has accelerated by approximately 19% compared to the period from 1983/84 to 2010 according to the same processing method.

Significant variability in decadal trends of C_{anth} accumulation has been observed, largely driven by its connection to the ocean's overturning circulation and related changes in the global carbon cycle (DeVries et al., 2017; Gruber, Clement, et al., 2019). This variability is also pronounced within individual ocean basins. In the Pacific Ocean, the C_{anth} inventory increased by 33% between 1995–2005 and 2005–2015 (Carter et al., 2019). Similarly, in the North Atlantic, the rate of C_{anth} storage doubled between the periods 1993–2003 and 2003–2014 (Wanninkhof et al., 2010; Woosley et al., 2016). Our previous work (Gao et al., 2022) also observed an acceleration in C_{anth} storage rates from the 1990s to the 2000s in the South Atlantic Ocean. The temporal variability in C_{anth} storage across regions is largely attributed to shifts in upper ocean ventilation with SAMW and AAIW playing critical roles in transporting C_{anth} into the ocean interior in the Southern Hemisphere. Our current findings demonstrate that C_{anth} accumulation has accelerated in the southeast Atlantic over the most recent decade. This acceleration, derived from both DIC and $\delta^{13}C$, contributes valuable insights to the ongoing discourse on decadal C_{anth} changes, which not only enhances our understanding of carbon uptake dynamics but also provide a foundation for exploring the relationship between C_{anth} accumulation and ocean ventilation processes.

4. Conclusions

The observed DIC change between 2010 and 2020 is much larger in the upper 500 m than in the deeper ocean layers within the narrow band of our study region in the southeastern Atlantic Ocean. However, the surface DIC increase is less than the expected DIC change based on atmospheric CO_2 increase, whereas the subsurface layer DIC is close to their respective air equilibrated values. In addition, the near surface (~10 m) oceanic Suess effect based on $\delta^{13}C$ observations is -0.24 ± 0.18‰ decade^{-1} between 2010 and 2020, which is close to that of the atmospheric $\delta^{13}C$ Suess effect (-0.25‰ decade^{-1}).

Based on both DIC and $\delta^{13}C$, ΔC_{anth} shows significant vertical differences and is highly dependent on water masses and circulation. Most of C_{anth} absorption is concentrated in the upper oceanic layers with an average ΔC_{anth} of 10.93 ± 1.45 μmol kg^{-1} in the SW, 8.11 ± 2.11 μmol kg^{-1} in the SAMW, and 4.11 ± 2.15 μmol kg^{-1} in the AAIW. Correspondingly, the signal of $\Delta\delta^{13}C_{anth}$ with relatively large changes also appears in SW (-0.30 ± 0.06‰), SAMW (-0.16 ± 0.05‰), and AAIW (-0.05 ± 0.03‰). These significant signals in both ΔC_{anth} and $\Delta\delta^{13}C_{anth}$ come from air-sea CO_2 exchange and formation and subduction of mode and intermediate waters. ΔC_{anth} is low in the deep waters with mean ΔC_{anth} of 1.16 ± 2.12 μmol kg^{-1} in the UCDW and 0.17 ± 0.66 μmol kg^{-1} in the LCDW and AABW, where the values of $\Delta\delta^{13}C_{anth}$ cluster around 0‰.

The RC values from Eide et al. (2017) and Quay et al. (2017) are used to convert $\Delta\delta^{13}C_{anth}$ to ΔC_{anth} and calculate CIC from $\Delta\delta^{13}C_{anth}$. Both DIC-based and $\delta^{13}C$-based estimations reveal similar anthropogenic carbon increase in the southeastern Atlantic Ocean over the most recent decade except for the SW. Moreover, the CIC values based on DIC and $\delta^{13}C$ show almost identical mean C_{anth} uptake rate (1.02 ± 0.32 vs. 1.00 ± 0.26 mol m^{-2} yr^{-1}) from 2010 to 2020, demonstrating that the results from the two methods are comparable. In addition, the C_{anth} uptake rate from 2010 to 2020 is faster than the rate between 1983/84 and 2010 when the exact same method is applied to DIC data.

Data Availability Statement

All the data are archived in publicly accessible databases. The data sets used in this study include cruises A12 in 2020 and A13.5 in 2010, which can be obtained from CLIVAR and Carbon Hydrographic Data Office (CCHDO, https://cchdo.ucsd.edu/). The A12 in 2020 is available from https://cchdo.ucsd.edu/cruise/33RO20200321, and A13.5 in 2010 is from https://cchdo.ucsd.edu/cruise/33RO20100308. Data are processed and analyzed with MATLAB R2024a (MathWorks, https://www.mathworks.com/products/matlab.html). The MATLAB codes used to perform data analysis and produce the manuscript's figures are available at https://github.com/huigao109/A13.5_d13C.

Acknowledgments
We are grateful to Dr. Rik Wanninkhof and Dr. Leticia Barbero for providing the ship opportunity and for sharing their DIC data with us. We thank the captains and crews for their efforts. We also thank Dr. Wanninkhof and Dr. Rolf Sonnerup for discussion. Finally, we thank the reviewers for their valuable feedback, which helped improve the quality of this work. We acknowledge financial support from NSF (OCE-2123768) to W-J.C.

References

Biastoch, A., Böning, C. W., & Lutjeharms, J. R. E. (2008). Agulhas leakage dynamics affects decadal variability in Atlantic overturning circulation. *Nature*, *456*(7221), 489–492. https://doi.org/10.1038/nature07426

Brewer, P. G. (1978). Direct observation of the oceanic CO_2 increase. *Geophysical Research Letters*, *5*(12), 997–1000. https://doi.org/10.1029/GL005i012p00997

Broecker, W. S., & Maier-Reimer, E. (1992). The influence of air and sea exchange on the carbon isotope distribution in the sea. *Global Biogeochemical Cycles*, *6*(3), 315–320. https://doi.org/10.1029/92GB01672

Broecker, W. S., & Peng, T. H. (1974). Gas exchange rates between air and sea. *Tellus*, *26*(1–2), 21–35. https://doi.org/10.3402/tellusa.v26i1-2.9733

Carter, B. R., Feely, R. A., Mecking, S., Cross, J. N., Macdonald, A. M., Siedlecki, S. A., et al. (2017). Two decades of Pacific anthropogenic carbon storage and ocean acidification along Global Ocean Ship-based Hydrographic Investigations Program sections P16 and P02. *Global Biogeochemical Cycles*, *31*(2), 306–327. https://doi.org/10.1002/2016GB005485

Carter, B. R., Feely, R. A., Wanninkhof, R., Kouketsu, S., Sonnerup, R. E., Pardo, P. C., et al. (2019). Pacific anthropogenic carbon between 1991 and 2017. *Global Biogeochemical Cycles*, *33*(5), 597–617. https://doi.org/10.1029/2018GB006154

Charles, C. D., Wright, J. D., & Fairbanks, R. G. (1993). Thermodynamic influences on the marine carbon isotope record. *Paleoceanography*, *8*(6), 691–697. https://doi.org/10.1029/93PA01803

Chen, G. T., & Millero, F. J. (1979). Gradual increase of oceanic CO_2. *Nature*, *277*(5693), 205–206. https://doi.org/10.1038/277205a0

Claret, M., Sonnerup, R. E., & Quay, P. D. (2021). A next generation ocean carbon isotope model for climate studies I: Steady state controls on ocean ^{13}C. *Global Biogeochemical Cycles*, *35*(4), e2020GB006757. https://doi.org/10.1029/2020GB006757

Clement, D., & Gruber, N. (2018). The eMLR (C*) method to determine decadal changes in the global ocean storage of anthropogenic CO_2. *Global Biogeochemical Cycles*, *32*(4), 654–679. https://doi.org/10.1002/2017GB005819

Deng, X., Li, Q., Su, J., Liu, C. Y., Atekwana, E., & Cai, W. J. (2022). Performance evaluations and applications of a $\delta^{13}C$-DIC analyzer in seawater and estuarine waters. *Science of the Total Environment*, *833*, 155013. https://doi.org/10.1016/j.scitotenv.2022.155013

DeVries, T., Holzer, M., & Primeau, F. (2017). Recent increase in oceanic carbon uptake driven by weaker upper-ocean overturning. *Nature*, *542*(7640), 215–218. https://doi.org/10.1038/nature21068

Eide, M., Olsen, A., Ninnemann, U. S., & Eldevik, T. (2017). A global estimate of the full oceanic ^{13}C Suess effect since the preindustrial. *Global Biogeochemical Cycles*, *31*(3), 492–514. https://doi.org/10.1002/2016GB005472

Friedlingstein, P., O'Sullivan, M., Jones, M. W., Andrew, R. M., Gregor, L., Hauck, J., et al. (2022). Global Carbon Budget 2022. *Earth System Science Data*, *14*(11), 4811–4900. https://doi.org/10.5194/essd-14-4811-2022

Friis, K., Körtzinger, A., Pätsch, J., & Wallace, D. W. (2005). On the temporal increase of anthropogenic CO_2 in the subpolar North Atlantic. *Deep Sea Research Part I: Oceanographic Research Papers*, *52*(5), 681–698. https://doi.org/10.1016/j.dsr.2004.11.017

Gao, H., Cai, W. J., Jin, M., Dong, C., & Timmerman, A. H. (2022). Ocean ventilation controls the contrasting anthropogenic CO_2 uptake rates between the western and eastern South Atlantic Ocean basins. *Global Biogeochemical Cycles*, *36*(6), e2021GB007265. https://doi.org/10.1029/2021GB007265

Gruber, N., Clement, D., Carter, B. R., Feely, R. A., Van Heuven, S., Hoppema, M., et al. (2019). The oceanic sink for anthropogenic CO_2 from 1994 to 2007. *Science*, *363*(6432), 1193–1199. https://doi.org/10.1126/science.aau5153

Gruber, N., Landschützer, P., & Lovenduski, N. S. (2019). The variable Southern Ocean carbon sink. *Annual Review of Marine Science*, *11*(1), 159–186. https://doi.org/10.1146/annurev-marine-121916-063407

Gruber, N., Sarmiento, J. L., & Stocker, T. F. (1996). An improved method for detecting anthropogenic CO_2 in the oceans. *Global Biogeochemical Cycles*, *10*(4), 809–837. https://doi.org/10.1029/96GB01608

Hauck, J., Hoppema, M., Bellerby, R. G. J., Völker, C., & Wolf-Gladrow, D. (2010). Data-based estimation of anthropogenic carbon and acidification in the Weddell Sea on a decadal timescale. *Journal of Geophysical Research*, *115*(C3), C03004. https://doi.org/10.1029/2009JC005479

Holte, J., Talley, L. D., Gilson, J., & Roemmich, D. (2017). An Argo mixed layer climatology and database. *Geophysical Research Letters*, *44*(11), 5618–5626. https://doi.org/10.1002/2017GL073426

Keeling, C. D. (1979). The Suess effect: 13Carbon-14Carbon interrelations. *Environment International*, *2*(4–6), 229–300. https://doi.org/10.1016/0160-4120(79)90005-9

Ko, Y. H., Lee, K., Quay, P. D., & Feely, R. A. (2014). Decadal (1994-2008) change in the carbon isotope ratio in the eastern South Pacific Ocean: Decadal $\delta^{13}C$ change in the South Pacific. *Global Biogeochemical Cycles*, *28*(8), 775–785. https://doi.org/10.1002/2013GB004786

Ko, Y. H., & Quay, P. D. (2020). Origin and accumulation of an anthropogenic CO_2 and ^{13}C Suess effect in the Arctic Ocean. *Global Biogeochemical Cycles*, *34*(2), e2019GB006423. https://doi.org/10.1029/2019GB006423

Körtzinger, A., Quay, P. D., & Sonnerup, R. E. (2003). Relationship between anthropogenic CO_2 and the ^{13}C Suess effect in the North Atlantic Ocean. *Global Biogeochemical Cycles*, *17*(1), 5-1–5-20. https://doi.org/10.1029/2001GB001427

Landschützer, P., Gruber, N., Haumann, F. A., Rödenbeck, C., Bakker, D. C., van Heuven, S., et al. (2015). The reinvigoration of the Southern Ocean carbon sink. *Science*, *349*(6253), 1221–1224. https://doi.org/10.1126/science.aab2620

McNeil, B. I., Matear, R. J., Key, R. M., Bullister, J. L., & Sarmiento, J. L. (2003). Anthropogenic CO_2 uptake by the ocean based on the global chlorofluorocarbon data set. *Science*, *299*(5604), 235–239. https://doi.org/10.1126/science.1077429

McNeil, B. I., Matear, R. J., & Tilbrook, B. (2001). Does carbon 13 track anthropogenic CO_2 in the Southern Ocean? *Global Biogeochemical Cycles*, *15*(3), 597–613. https://doi.org/10.1029/2000GB001352

Mook, W. G., Bommerson, J. C., & Staverman, W. H. (1974). Carbon isotope fractionation between dissolved bicarbonate and gaseous carbon dioxide. *Earth and Planetary Science Letters*, *22*(2), 169–176. https://doi.org/10.1016/0012-821X(74)90078-8

Müller, J. D., Gruber, N., Carter, B., Feely, R., Ishii, M., Lange, N., et al. (2023). Decadal trends in the oceanic storage of anthropogenic carbon from 1994 to 2014. *AGU Advances*, *4*(4), e2023AV000875. https://doi.org/10.1029/2023AV000875

Olsen, A., & Ninnemann, U. (2010). Large $\delta^{13}C$ gradients in the preindustrial North Atlantic revealed. *Science*, *330*(6004), 658–659. https://doi.org/10.1126/science.1193769

Olsen, A., Omar, A. M., Bellerby, R. G., Johannessen, T., Ninnemann, U., Brown, K. R., et al. (2006). Magnitude and origin of the anthropogenic CO_2 increase and ^{13}C Suess effect in the Nordic seas since 1981. *Global Biogeochemical Cycles*, *20*(3), GB3027. https://doi.org/10.1029/2005GB002669

Orselli, I. B., Kerr, R., de Azevedo, J. L., Galdino, F., Araujo, M., & Garcia, C. A. (2019). The sea-air CO_2 net fluxes in the South Atlantic Ocean and the role played by Agulhas eddies. *Progress in Oceanography*, *170*, 40–52. https://doi.org/10.1016/j.pocean.2018.10.006

Orsi, A. H., Whitworth, III, T., & Nowlin, W. D., Jr. (1995). On the meridional extent and fronts of the Antarctic Circumpolar Current. *Deep Sea Research Part I: Oceanographic Research Papers*, *42*(5), 641–673. https://doi.org/10.1016/0967-0637(95)00021-W

Pardo, P. C., Pérez, F. F., Khatiwala, S., & Ríos, A. F. (2014). Anthropogenic CO_2 estimates in the Southern Ocean: Storage partitioning in the different water masses. *Progress in Oceanography*, *120*, 230–242. https://doi.org/10.1016/j.pocean.2013.09.005

Quay, P., Sonnerup, R., Munro, D., & Sweeney, C. (2017). Anthropogenic CO_2 accumulation and uptake rates in the Pacific Ocean based on changes in the $^{13}C/^{12}C$ of dissolved inorganic carbon. *Global Biogeochemical Cycles*, *31*(1), 59–80. https://doi.org/10.1002/2016GB005460

Quay, P., Sonnerup, R., Stutsman, J., Maurer, J., Körtzinger, A., Padin, X. A., & Robinson, C. (2007). Anthropogenic CO_2 accumulation rates in the North Atlantic Ocean from changes in the $^{13}C/^{12}C$ of dissolved inorganic carbon. *Global Biogeochemical Cycles*, *21*(1), GB1009. https://doi.org/10.1029/2006GB002761

Quay, P., Sonnerup, R., Westby, T., Stutsman, J., & McNichol, A. (2003). Changes in the $^{13}C/^{12}C$ of dissolved inorganic carbon in the ocean as a tracer of anthropogenic CO_2 uptake. *Global Biogeochemical Cycles*, *17*(1), 4-1–4-20. https://doi.org/10.1029/2001GB001817

Quay, P. D., Tilbrook, B., & Wong, C. S. (1992). Oceanic uptake of fossil fuel CO_2: Carbon-13 evidence. *Science*, *256*(5053), 74–79. https://doi.org/10.1126/science.256.5053.74

Racapé, V., Pierre, C., Metzl, N., Lo Monaco, C., Reverdin, G., Olsen, A., et al. (2013). Anthropogenic carbon changes in the Irminger Basin (1981–2006): Coupling δ^{13}CDIC and DIC observations. *Journal of Marine Systems*, *126*, 24–32. https://doi.org/10.1016/j.jmarsys.2012.12.005

Sabine, C. L., Feely, R. A., Gruber, N., Key, R. M., Lee, K., Bullister, J. L., et al. (2004). The oceanic sink for anthropogenic CO_2. *Science*, *305*(5682), 367–371. https://doi.org/10.1126/science.1097403

Sabine, C. L., Feely, R. A., Millero, F. J., Dickson, A. G., Langdon, C., Mecking, S., & Greeley, D. (2008). Decadal changes in Pacific carbon. *Journal of Geophysical Research*, *113*(C7), C07021. https://doi.org/10.1029/2007JC004577

Sabine, C. L., Key, R. M., Johnson, K. M., Millero, F. J., Poisson, A., Sarmiento, J. L., et al. (1999). Anthropogenic CO_2 inventory of the Indian Ocean. *Global Biogeochemical Cycles*, *13*(1), 179–198. https://doi.org/10.1029/1998GB900022

Sallée, J. B., Matear, R. J., Rintoul, S. R., & Lenton, A. (2012). Localized subduction of anthropogenic carbon dioxide in the Southern Hemisphere oceans. *Nature Geoscience*, *5*(8), 579–584. https://doi.org/10.1038/ngeo1523

Schmittner, A., Gruber, N., Mix, A. C., Key, R. M., Tagliabue, A., & Westberry, T. K. (2013). Biology and air–sea gas exchange controls on the distribution of carbon isotope ratios (δ^{13}C) in the ocean. *Biogeosciences*, *10*(9), 5793–5816. https://doi.org/10.5194/bg-10-5793-2013

Sonnerup, R. E., Mcnichol, A. P., Quay, P. D., Gammon, R. H., Bullister, J. L., Sabine, C. L., & Slater, R. D. (2007). Anthropogenic δ^{13}C changes in the North Pacific Ocean reconstructed using a multiparameter mixing approach (MIX). *Tellus B: Chemical and Physical Meteorology*, *59*(2), 303. https://doi.org/10.1111/j.1600-0889.2007.00250.x

Sonnerup, R. E., & Quay, P. D. (2012). ^{13}C constraints on ocean carbon cycle models. *Global Biogeochemical Cycles*, *26*(2), GB2014. https://doi.org/10.1029/2010GB003980

Sonnerup, R. E., Quay, P. D., & McNichol, A. P. (2000). The Indian Ocean ^{13}C Suess effect. *Global Biogeochemical Cycles*, *14*(3), 903–916. https://doi.org/10.1029/1999GB001244

Su, J., Cai, W. J., Hussain, N., Brodeur, J., Chen, B., & Huang, K. (2019). Simultaneous determination of dissolved inorganic carbon (DIC) concentration and stable isotope (δ^{13}C-DIC) by Cavity Ring-Down Spectroscopy: Application to study carbonate dynamics in the Chesapeake Bay. *Marine Chemistry*, *215*, 103689. https://doi.org/10.1016/j.marchem.2019.103689

Sun, Z., Li, X., Ouyang, Z., Featherstone, C., Atekwana, E. A., Hussain, N., & Cai, W. (2024). Simultaneous onboard analysis of seawater dissolved inorganic carbon (DIC) concentration and stable isotope ratio (δ^{13}C-DIC). *Limnology and Oceanography: Methods*, 10642. https://doi.org/10.1002/lom3.10642

Talley, L. D. (2011). *Descriptive physical oceanography: An introduction*. Academic Press.

Tanhua, T., Körtzinger, A., Friis, K., Waugh, D. W., & Wallace, D. W. R. (2007). An estimate of anthropogenic CO_2 inventory from decadal changes in oceanic carbon content. *Proceedings of the National Academy of Sciences*, *104*(9), 3037–3042. https://doi.org/10.1073/pnas.0606574104

Touratier, F., & Goyet, C. (2004). Definition, properties, and Atlantic Ocean distribution of the new tracer TrOCA. *Journal of Marine Systems*, *46*(1–4), 169–179. https://doi.org/10.1016/j.jmarsys.2003.11.020

Ulfsbo, A., Jones, E. M., Casacuberta, N., Korhonen, M., Rabe, B., Karcher, M., & Van Heuven, S. M. A. C. (2018). Rapid changes in anthropogenic carbon storage and ocean acidification in the intermediate layers of the Eurasian Arctic Ocean: 1996–2015. *Global Biogeochemical Cycles*, *32*(9), 1254–1275. https://doi.org/10.1029/2017GB005738

van Heuven, S., Pierrot, D., Lewis, E., & Wallace, D. W. R. (2011). *MATLAB program developed for CO_2 system calculations, ORNL/CDIAC-105b*. Carbon Dioxide Information Analysis Center, Oak Ridge National Laboratory, U.S. Department of Energy.

Vázquez-Rodríguez, M., Padin, X. A., Ríos, A. F., Bellerby, R. G. J., & Pérez, F. F. (2009). An upgraded carbon-based method to estimate the anthropogenic fraction of dissolved CO_2 in the Atlantic Ocean. *Biogeosciences Discussions*, *6*(2), 4527–4571. https://doi.org/10.5194/bgd-6-4527-2009

Wallace, D. (1995). *Monitoring global ocean carbon inventories* (p. 54). Ocean Observing System Development Panel, Texas A&M University.

Wanninkhof, R., Doney, S. C., Bullister, J. L., Levine, N. M., Warner, M., & Gruber, N. (2010). Detecting anthropogenic CO_2 changes in the interior Atlantic Ocean between 1989 and 2005. *Journal of Geophysical Research*, *115*(C11), C11028. https://doi.org/10.1029/2010JC006251

Williams, T. J., Wagner, A. J., Sikes, E. L., & Martin, E. E. (2021). Evolution of the oceanic ^{13}C Suess effect in the southeastern Indian Ocean between 1994 and 2018. *Geochemistry, Geophysics, Geosystems*, *22*(4), e2020GC009402. https://doi.org/10.1029/2020GC009402

Woosley, R. J., Millero, F. J., & Wanninkhof, R. (2016). Rapid anthropogenic changes in CO_2 and pH in the Atlantic Ocean: 2003–2014. *Global Biogeochemical Cycles*, *30*(1), 70–90. https://doi.org/10.1002/2015GB005248

Zhang, J., Quay, P. D., & Wilbur, D. O. (1995). Carbon isotope fractionation during gas-water exchange and dissolution of CO_2. *Geochimica et Cosmochimica Acta*, *59*(1), 107–114. https://doi.org/10.1016/0016-7037(95)91550-D

References From the Supporting Information

Maritorena, S., d'Andon, O. H. F., Mangin, A., & Siegel, D. A. (2010). Merged satellite ocean color data products using a bio-optical model: Characteristics, benefits and issues. *Remote Sensing of Environment*, *114*(8), 1791–1804. https://doi.org/10.1016/j.rse.2010.04.002

Maritorena, S., & Siegel, D. A. (2005). Consistent merging of satellite ocean color data sets using a bio-optical model. *Remote Sensing of Environment*, *94*(4), 429–440. https://doi.org/10.1016/j.rse.2004.08.014

Nash, J. E., & Sutcliffe, J. V. (1970). River flow forecasting through conceptual models part I—A discussion of principles. *Journal of Hydrology*, *10*(3), 282–290. https://doi.org/10.1016/0022-1694(70)90255-6